3D printed auto-mixing chip enables rapid smartphone diagnosis of anemia

Kimberly Plevniak,[1] Matthew Campbell,[2] Timothy Myers,[3] Abby Hodges,[3] and Mei He[1,4,a)]

[1]*Department of Biological and Agricultural Engineering, Kansas State University, Manhattan, Kansas 66506, USA*
[2]*Advanced Manufacturing Institute, Kansas State University, Manhattan, Kansas 66506, USA*
[3]*Department of Science and Mathematics, MidAmerica Nazarene University, Olathe, Kansas 66062, USA*
[4]*Terry C. Johnson Cancer Research Center, Kansas State University, Manhattan, Kansas 66506, USA*

(Received 30 July 2016; accepted 26 September 2016; published online 5 October 2016)

Clinical diagnosis requiring central facilities and site visits can be burdensome for patients in resource-limited or rural areas. Therefore, development of a low-cost test that utilizes smartphone data collection and transmission would beneficially enable disease self-management and point-of-care (POC) diagnosis. In this paper, we introduce a low-cost *i*POC^{3D} diagnostic strategy which integrates 3D design and printing of microfluidic POC device with smartphone-based disease diagnosis in one process as a stand-alone system, offering strong adaptability for establishing diagnostic capacity in resource-limited areas and low-income countries. We employ smartphone output (AutoCAD 360 app) and readout (color-scale analytical app written in-house) functionalities for rapid 3D printing of microfluidic auto-mixers and colorimetric detection of blood hemoglobin levels. The auto-mixing of reagents with blood via capillary force has been demonstrated in 1 second without the requirement of external pumps. We employed this *i*POC^{3D} system for point-of-care diagnosis of anemia using a training set of patients ($n_{anemia} = 16$ and $n_{healthy} = 6$), which showed consistent measurements of blood hemoglobin levels (a.u.c. = 0.97) and comparable diagnostic sensitivity and specificity, compared with standard clinical hematology analyzer. Capable of 3D fabrication flexibility and smartphone compatibility, this work presents a novel diagnostic strategy for advancing personalized medicine and mobile healthcare. *Published by AIP Publishing.* [http://dx.doi.org/10.1063/1.4964499]

INTRODUCTION

Microfluidic point-of-care (POC) diagnosis is an emerging field for advancing healthcare accessibility and affordability, which offers prompt results, timely interventions, and improved efficacy.[1–5] Presently, 3D printing technology has been involved and showed tremendous potential for developing microfluidic POC devices, owing to the low-cost, fast and one-step fabrication capability, without the need of laboratory resources.[6–8] Traditional microfabrication of low-cost polymer-based (e.g., Polydimethylsiloxane (PDMS)) microfluidic POC devices requires lithographic fabrication of molds to replicate PDMS POC chips.[9,10] The paper-based microfluidic devices are sensitive to environmental conditions (e.g., humidity) and not durable.[11,12] In contrast, a consumer-grade 3D printer can produce highly versatile, durable microfluidic POC devices without the need of laboratory settings.[13–16] Application of 3D printing in microfluidic technology has shown tremendous potential in tissue engineering,[17–19] sample preparation

a)Author to whom correspondence should be addressed. Electronic mail: meih@ksu.edu

techniques,[20] and cell processing.[21–24] Zhang *et al.* introduced a 3D printed microfluidic chip which utilizes a water and oil interface to filter out the lysate contaminants for extraction of nucleic acids.[20] Chan *et al.* developed movable 3D printed microfluidic chip components, such as torque-actuated pump and valve, rotary valve, and pushing valve, for assembling microfluidic POC devices.[25] The tedious, multiple 3D printed components need to be assembled and employed for protein quantification from artificial urine samples with a smartphone as an imaging platform. The 3D printer also has been frequently used for making parts that serve smartphone optical interfaces.[26–29] Filippini research group has done pioneer work in developing unibody Lab on a Chip (LOC) chip which integrates 3D printed parts as microfluidic POC device with smartphone sensing.[30,31] In spite of being a variable and powerful technology, applications of a 3D printer in microfluidic POC diagnosis with smartphone as a stand-alone system are still needed to be explored more broadly.[32] Herein, we introduce a simple and low-cost approach that integrates 3D design and printing of monolithic microfluidic mixers with smartphone-based diagnosis in one process, for developing a stand-alone diagnostic system (*i*POC^{3D} system).

We demonstrated *i*POC^{3D} system for POC diagnosis of anemia. Anemia often causes high fetal mortality and abnormalities, premature deaths, low birth weights for infants, and retarded brain development, which affects over half of pre-school children and pregnant women in developing countries.[33,34] Although anemia screening is highly recommended for infants and pregnant women by the U.S. Preventive Services Task Force and other developing countries, the bottleneck in control of anemia falls on the accessible screening tools needed to eliminate distance barriers.[35] Clinical diagnosis of anemia by measuring blood hemoglobin (Hgb) levels in rural areas or low-income countries is facing substantial logistic challenges, due to the difficulties in maintaining frequent and costly medical visits. Oftentimes, blood hemoglobin levels need to be known immediately for making decision of blood transfusion at the point of care.[36] Therefore, a stand-alone POC diagnostic system for screening anemia is needed for solving such logistic channelings.

We employ smartphone output (AutoCAD 360 app) and readout (color-scale analytical app written in-house) functionalities for rapid 3D printing of microfluidic auto-mixer and colorimetric detection of blood hemoglobin levels. In addition to generating a POC microfluidic device, the 3D printer can produce a POC chip housing to align with the smartphone camera and optical lens (Fig. 1). The 3D microfluidic simulation was studied to guide computer design and prototyping of POC devices, thereby enabling rapid optimization of various geometries and microstructures for improving mixing performance as needed. The auto-mixing of reagents with blood via capillary force was demonstrated in 1 s for the first time. Without requiring laboratory setup and external off-chip operation (e.g., pump), 3D printed monolithic microfluidic auto-

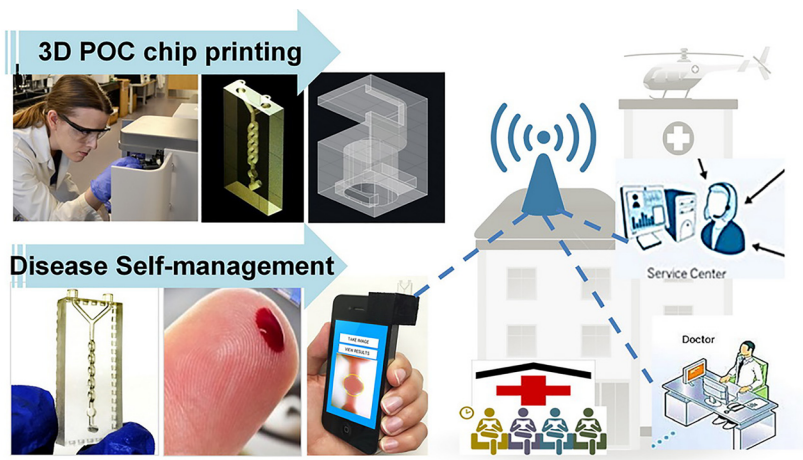

FIG. 1. Low-cost, smartphone-based, 3D-printed POC microfluidic chip (smartphone *i*POC^{3D} system) for rapid diagnosis of anemia in 60 s.

mixer can introduce oxidizing agents with blood for fast mixing and bioreaction, allowing finger prick blood (~5 μl) assay of hemoglobin levels. Integrated with smartphone image analysis and data transmission (color-scale analytical app written in-house), self-management and POC diagnosis of anemia was successfully implemented, showing consistent results with clinical measurements and good diagnostic accuracy (a.u.c. = 0.97) from testing a training set of anemia patients. Hereby, we introduce a low-cost diagnostic strategy (*i*POC^{3D}) which enables microfluidic POC device design and fabrication, and disease management integrated in one process as a standalone system, offering strong adaptability for establishing diagnostic capacity in resource-limited areas and low-income countries. Our pilot study, focused on anemia diagnosis, represents a key step towards developing variable and advanced mobile healthcare tests which eliminate the expenses of clinic visits and facility resources.

MATERIALS AND METHODS

3D printing of microfluidic chip

Three-dimensional design is always difficult within conventional microfabrication, due to complicated protocols for accurate alignment and multilayer bonding. Configured with smartphone solid modeling app (AutoCAD 360), we used a laptop-sized 3D printer (D3 ProJet 1200, 30-μm resolution) for fabrication of monolithic microfluidic chips. VisiJet® FTX Clear resin consisting of triethylene glycol diacrylate, sobornyl methacrylate, and 2%–3% photoinitiator phenylbis (2,4,6-trimethylbenzoyl)-phosphine oxide was used to produce transparent 3D microfluidic chips per vendor's instruction. Printed 3D devices were cleaned using isopropyl alcohol and blown dry. The uncured resin within the microchannel was flushed out by an air compressor. A field emission scanning electron microscope (SEM) characterized printed microstructures using a focus ion beam (FEI Versa) after gold sputtering coating in 20-nm thickness. Ethylene glycol chemistry was used to develop the hydrophilic surface of 3D printed devices: 1.82 M potassium hydroxide (KOH) was mixed into pure ethylene glycol solution (Sigma-Aldrich; anhydrous, 99.8%) and used to soak 3D devices at 55 °C for 2 h. When needed, we can also bond the 3D printed objects with glass materials when 3% of photoinitiator 2-(2-bromoisobutyryloxy)ethyl methacrylate (BrMA, Sigma-Aldrich) was introduced into clear resin and mixed. The Silane-Prep glass slides pretreated with aminoalkylsilane (Sigma-Aldrich) were used to bond the 3D printed layer with open channels and microstructures. The clean 3D layer annealed very well with the glass slides. The two annealed layers were then exposed to 365-UV for 8 min. The bonding was irreversible via covalent chemical bond.

Auto-mixing assay development

3D computational fluid dynamic (CFD) simulations were performed using ANSYS CFX (R16.1) to guide microfluidic design and achieve effective capillary-driven auto-mixing in the microfluidic mixer. The simulation parameters and conditions are detailed in the supplementary material. The visual readout for anemia diagnosis from the view-window in which blood mixed with the reagents was based on the 3,3′,5,5′-tetramethylbenzidine (TMB) (Sigma-Aldrich) and hydrogen peroxide (H_2O_2) (Sigma-Aldrich) oxidation-reduction reaction with hemoglobin as a catalyst. The amount of hemoglobin determined the charge transfer status of TMB, which was displayed in various colors. The 1:1 volume ratio of blood (10 times dilution) and reagents was developed to gauge an assay using 5 μl of finger-prick blood. Consistent sample introduction was ensured by using a 3D printed sampling well with "slot-in" placement of chips (see details in the supplementary material).

Smartphone output and readout

An android phone with AutoCAD 360 app was configured with the 3D printer for wireless transmitting solid modeling design. The android phone camera was used for collecting assay readout through a color-scale analytical app written in-house. A 3D printed POC chip housing with a 5× gel lens on camera was assembled for capturing and analyzing color-scale results from

the chip view-window (Fig. 1). Color-scale image capture and analysis app written in-house was developed to extract RGB (red, green, and blue) peak values in the region of interest (ROI) in the view-window. RGB peak values were then converted to CIE L*a*b* color space values corresponding to Hgb concentrations via calibration, using the MATLAB mathematic model.[37] The CIE L*a*b* color space is a color representation model which maps a three-dimensional integer space for device-independent digital representation of color.[37]

Clinical blood samples

Study protocols and clinical sample collection protocols were approved by the IRB committee of Kansas State University and the University of Kansas Medical Center and Hospital. The inclusion criteria include aged 25–39 years on the day of inclusion and resident of the site zone, and being able to attend anemia screening (no exclusion criteria). A total of 22 clinical blood samples from adult patients and healthy donors in outpatient clinics of the University of Kansas Hospital and Biorepository were collected, tested, and analyzed using our smartphone *i*POC^{3D} system (see details in the supplementary material). All samples were acquired under informed consent. Results from smartphone *i*POC^{3D} system were compared with patients' clinical Complete Blood Count (CBC) tests which measure the hemoglobin levels by hematology analyzer through 2 ml of venous blood draw. The study revealed that patients benefited from much less blood sampling and rapid data readout.

RESULTS AND DISCUSSIONS

Principle and 3D simulation for capillary-driven auto-mixing

Flow behavior in several 3D microfluidic channels and microstructures were studied in order to develop an effective capillary force driven auto-mixing in a 3D printed microfluidic mixer. The flow in microfluidic channels is characterized by low Reynold's numbers, which indicates that the flow regime is laminar. For incompressible, laminar flow in a circular microscale tube (microfluidic channels), the flow can be represented by the Hagen–Poiseuille equation.[38] The surface tension forces (capillary force) and the viscous forces (frictional drag) are the governing forces,[39] and the gravitational force can be ignored due to low bond (Bo) number in microscale tube.[40] Thus, the auto-mixing flow rate is determined by a force balance between the capillary force and the frictional force. The capillary force can be represented by the below equation by the principle of Young–Laplace[41]

$$\Delta P = \frac{4\sigma \cos\theta}{D},$$

where ΔP is the pressure drop, σ is the surface tension, θ is the contact angle, and D is the channel diameter. The frictional drag force for laminar flow in a round channel can be represented by[42]

$$\Delta P = \frac{64}{Re} \times \frac{L}{D} \times \frac{\bar{V}^2}{2} \times \rho,$$

where Re is the Reynold's number (ρVD/μ),[43] μ is the dynamic viscosity of the fluid, L is the wetted length, V is the flow velocity, and ρ is the density. By equating frictional force to capillary force based on the above two equations, we can determine the auto-mixing velocity by the following relation:

$$\bar{V} = \frac{D\sigma \cos\theta}{8\mu L}.$$

Therefore, the capillary-force induced flow rate is governed by geometry, surface properties, and fluid profile properties. At a given fluid, geometry or characteristic dimension of

microfluidic channel in given surface chemistry dominates the capillary-force induced flow rate. The velocity of capillary flow is fast at short wetted lengths while slow at long wetted lengths. Contact angle affects the capillary flow rate under varied surface conditions (e.g., chemistry and roughness) (see Figure S1 of the supplementary material) with higher flow rate induced by smaller contact angle. The flow rate will increase with larger channel diameters, until gravitational force and inertial forces become dominant. On the other hand, at small diameters, the flow rate tends to be extremely slow due to the drag force overpowering the surface force. Hence, the theoretical analysis gives an applicable dimension regime of microchannels for a capillary force driven flow, ranging from ∼100 μm to 2 mm in diameter with Reynold's numbers below 500. The typical capillary flow rate in a microchannel with 500 μm in diameter and 22 mm in wetted length is about 20 μl/s.

We initially designed three microfluidic mixers with characteristic size of 500 μm in microchannel diameter: split and recombination (SAR) (Fig. 2(a)), serpentine channel (Fig. 2(b)), and ring channel (Fig. 2(c)). All three of these designs have Bo numbers less than 1, indicating that capillary force is dominant, and have Reynold's numbers ranging from 11 to ∼450. A Y-shaped channel was used to introduce the two flows into the mixing unit and a round circular chamber served as a view-window. The SAR micromixer was adapted from published work by Lee *et al.*[44] who fabricated the SAR device using PDMS by complicated multilayer alignment and bonding. In contrast, we fabricated the SAR device by one-touch 3D printing. In the SAR micromixer, the split and recombination process increased flow interfaces exponentially by continually laminating interfaces along the channel, resulting in fluidic mixing. Although serpentine channel is a classic design[45] used for microfluidic mixing, the basic serpentine is not suitable for fast mixing, due to diffusion dominated mixing process which requires relatively longer mixing time. By combing the split and recombination structure with the serpentine structure, we designed a ring-shaped mixing channel (Fig. 2(c)).

We established a CFD model to simulate blood flow mixed with aqueous solution under capillary force in three micromixers (see details in the supplementary material). As shown in Fig. 2(d) straight flow-through channel, the two flows were unable to mix. The sharp boundary between the two flows demonstrated the time frame for diffusive mixing which was much longer than the fluid residence time at the given capillary driven flow rate. By inclusion of the SAR units in the straight flow-through channel, blood flow can mix completely with the

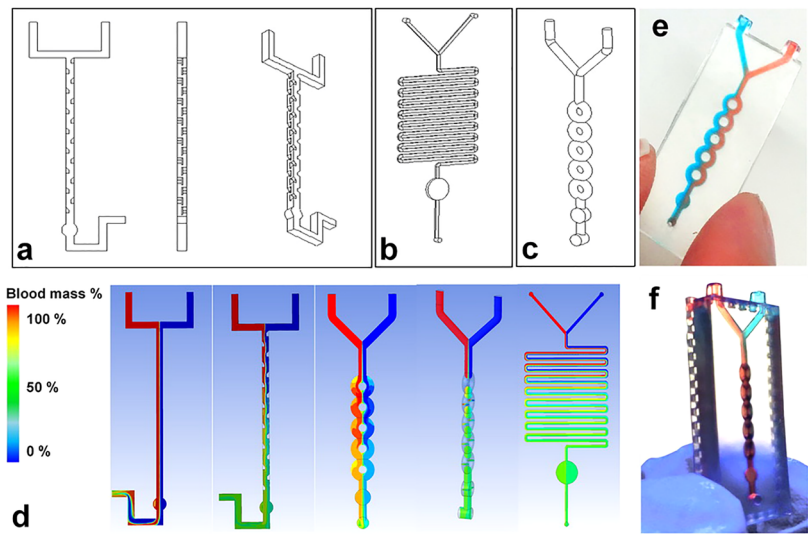

FIG. 2. Design of three microfluidic mixers: (a) SAR, (b) serpentine channel, and (c) ring-shaped channel. Channel diameter was ∼500 μm. (d) 3D CFD simulation of blood mixing profile in three micromixers: Red flow is blood mixed with aqueous solution (blue); green color indicates complete mixing. (e) Experimental image of 3D printed planner micromixer showing incomplete mixing under capillary force using colored dye solutions. (f) Experimental image of 3D printed, 3D-structured micromixer showing efficient mixing within 1 s using colored dye solutions.

aqueous solution after passing into the view-window of the SAR micromixer. We also simulated the blood mixing profile in ring-shaped micromixer. Although ring channel directed the flow to split and recombine, two flows were unable to crossover, and continue to flow side-by-side. The initial simulation results led us to a novel design by rotating the ring structure 90° in the x-y plane with respect to the "Y" inlet (see Fig. 2(d), fourth figure). Thus, two flows can be split in a manner that causes interfaces to travel through the ring section. Due to the large amount of chaotic advection occurring in the ring channels, fast mixing (∼1 s) can be achieved in a more compact 3D micro-structure. Along with the supplementary CFD simulation videos 1 and 2 (see supplementary material), the rapid prototyping was demonstrated in Figs. 2(e) and 2(f). We used food dyes in red and blue to experimentally demonstrate the auto-mixing process, and the experimental results are consistent with the simulation results (Figs. 2(e) and 2(f)). For serpentine micromixer, due to the long channel length (∼255 mm), the capillary-driven flow rate was relatively slow and required more time for fluids to flow through the device (∼1 min), which consequently provides ample time for diffusive mixing. On the contrary, the SAR and ring micromixers have relatively short lengths (∼30 mm and 22 mm), resulting in high capillary-driven flow rates and shorter mixing times (less than a second). In order to develop quick mixing of blood with reagents, we chose the rotated ring channel micromixer for following tests.

Fabrication of 3D microfluidic POC chips

SEM imaging was performed to characterize 3D printing quality. Wireless printing was conducted through desktop size D3 ProJet 1200 3D printer which has a build area of 43 mm × 27 mm × 150 mm and provides a physical pixel size of 56 μm × 30 μm. After the printing was complete, the 3D object was washed with isopropyl alcohol, and uncured resin was flushed out by an air compressor. We printed a number of basic structures and three micromixer designs to evaluate printing capability and quality, as shown in Fig. 3. The SAR micromixer with eight mixing units was readily printed out in less than 10 min, and the chip was completely transparent for visualizing colored reagents in the microchannel (Fig. 3(a)). Note that the PDMS-fabricated SAR micromixer requires complicated alignment and multilayer bonding, which takes more than one day to complete. The rotated, ring-shaped channels were prototyped in 10 min, without requiring additional equipment, as shown by the angled view in Fig. 3(b). The serpentine channel was also successfully printed, as shown by SEM imaging in Fig. 3(c). A smooth surface was observed in the microchannel and circular chamber. Other basic structures often used in microfluidic chips were also characterized, including post arrays (Figs. 3(d) and 3(e)), microwells (Fig. 3(f)), and a D-shaped hollow microchannel. The cost for printing each 3D microfluidic chip is less than 50 cents. Close examination of SEM images

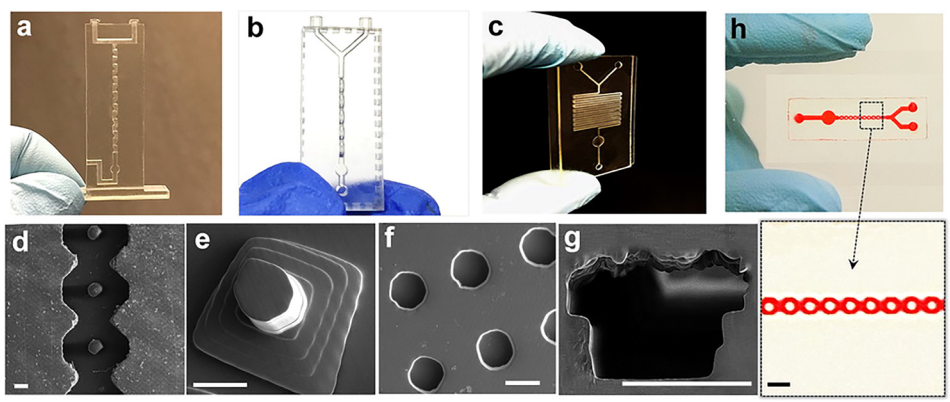

FIG. 3. Characterization of 3D printing for fabricating microfluidic mixers: (a) SAR microfluidic mixer, (b) 3D ring-shaped micromixer, (c) and serpentine micromixer. Channel diameter is ∼500 μm. SEM imaging was used to characterize variable 3D-printed microstructures: (d) posts in curved microfluidic channel, (e) pyramid post arrays, (f) microwells, and (g) a D-shaped hollow microchannel. Scale bar: 200 μm. (h) The bonded layer of a 3D-printed open channel with a glass slide.

revealed additional printing properties, and printing layers were observed due to the minimum pixel resolution (30 μm), such as the "stair"-looking of the D-shaped microchannel shown in Fig. 3(g) (diameter of 200 μm). Although a smaller channel could be printed, complete removal of uncured resin was difficult, due to high backpressure for cleaning.[13]

We also developed a bonding protocol to attach a 3D printed open channel layer to a glass slide (Fig. 3(h)). An open channel with a diameter of 50 μm can be printed and attached to a glass slide, resulting in a closed hollow microchannel. The bonding protocol follows the principle of saline chemistry by forming covalent chemical bonds between the glass surface and resin surface. As shown in Fig. 3(h), the ring-shaped channel in 50-μm deep and wide was bonded to a glass slide without leakage observed, which was proven by running through a red dye solution. This protocol could extend the 3D printer capability for printing smaller hollow microchannels below 200 μm i.d.

The cured resin was slightly hydrophobic, as indicated by measuring contact angles (Fig. 4(a), $\theta = 64°$), so we developed a simple chemistry protocol for treating 3D printed objects into hydrophilic property. The 3D printed micromixer chip was immersed into a pure ethylene glycol solution containing 1.82 M KOH and incubated at 55 °C for 2 h.[46] The contact angle of deionized (DI) water was measured to note the hydrophilicity of 3D printed microfluidic chip as compared with PDMS and glass materials. As shown in Fig. 4(a), hydrophilicity was significantly improved ($\theta = 32°$, RSD = 4.6%, and n = 10), providing a stable capillary-driven force for auto-mixing. Hydrophilically treated 3D chip also can be stored in water solution for reuse for several days, thereby maintaining a stable surface chemistry. We further characterized the surface chemistry using Fourier transform infrared spectroscopy (FTIR). Untreated surface spectra failed to show an OH stretch between 3000 and 3750 cm^{-1} (Fig. 4(b)) compared with treated 3D printing material which exhibits strong OH stretches. Such hydrophilic surface provides a stable capillary force required for auto-mixing of blood with test reagents.

Rapid POC diagnosis of anemia

Utilizing capillary-driven auto-mixing in a 3D-printed microfluidic mixer, we developed a color-scale assay for POC diagnosis and self-management of anemia. Hemoglobin (Hgb) level is the primary laboratory parameter for the clinical diagnosis of anemia.[47] The current gold standard is a complete blood count (CBC) using a hematology analyzer via venous blood, which requires a blood draw by a trained phlebotomist and needs electrical power to operate in centralized hospitals or clinics.[48] Several portable devices for anemia diagnosis have been developed,[49,50] such as HemoCue-B Hemoglobin,[51] STAT-Site® MHgb,[52] Rainbow® signal extraction technology (SET), and SpectOLight™ Occlusion.[53] However, few of these tools are well-suited for transferring to low-resource areas, due to their costs and sophisticated designs that require professional operation. Simple and disposable platforms have recently been developed to test blood Hgb levels,[37,54,55] including the WHO Hb color scale (HbCS) test,[56] but these platforms require fabrication facilities in scientific laboratories or skilled technicians for mass production and technology transfer, thereby offering limited adaptability for establishing study capacity in rural areas or low-income countries.

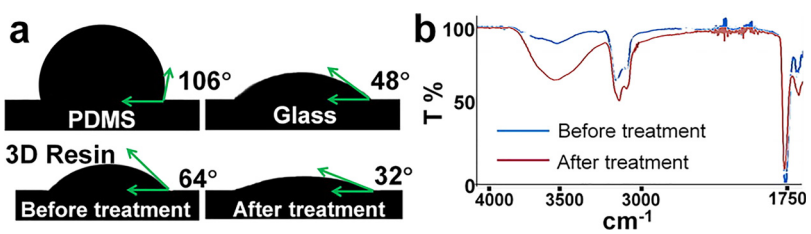

FIG. 4. (a) Hydrophilic surface treatment of 3D-printed microfluidic chip for capillary-driven auto-mixing; the contact angle (θ) of DI water shows the hydrophilicity of PDMS, glass, and printed resin before and after treatment. (b) FTIR analysis of surface chemistry of 3D printed resin before and after surface treatment.

We developed a color-scale assay combined with smartphone to ascertain Hgb blood levels using only ∼5 μl blood from a finger prick. The diluted drop of blood and oxidizing agents were hold uniformly and tightly in micro-wells (∼20 μl volume) in 3D printed sampling platform, due to the surface tension (Fig. 5(a)). Therefore, consistent sample introduction was ensured by using a "slot-in" placement of chips in this sampling platform (Fig. 5(b)). The sampling platform also can be printed as an array format. The visual readout via smartphone camera from the micromixer reaction chamber was based on the 3,3′,5,5′-TMB oxidation-reduction reaction with blood Hgb as a catalyst. The amount of Hgb determines the charge transfer status of TMB (charge transfer TMB complex with one-electron is in blue and two-electrons is in yellow).[37,57] Excess hemoglobin yields a red color. Thus, depending on the ratio of several color species in the mixture, the resultant visual colors span blue, green, yellow, orange, and red with increased hemoglobin concentration (Figs. 5(c) and 5(d)). The color images collected from an android phone with a micromixer housing system were consistently obtained in order to define ROI and quantitative RGB analysis. We used a rotated ring channel design to rapidly mix blood with the oxidizing agents in 1 s and observe color development. The standard hemoglobin protein was spiked in 100-time diluted blood with concentrations of 0, 5.5, 8.0, 9.0, 12.5, and 16.0 g/dL, which was used to establish a calibration curve for correlating color-scales ($R^2 = 0.99$ and RSD = ∼2.5%−5%; Fig. 5(d)). The visual readout from the micromixer was also calibrated by comparing with photospectrometer measurements for quantitative measurement of Hgb concentrations (Fig. 5(e)). Absorbance peaks of Hgb at 540 nm and 575 nm showed linear increase with increased Hgb concentrations. In contrast, the absorbance peak of TMB at 630 nm decreased with high Hgb levels due to TMB oxidization. The analysis of blood from a healthy donor showed Hgb level in line with the WHO recommended cutoff as a positive reference.

In order to further validate the clinical usability of developed smartphone *i*POC^{3D} system, we started a clinical training set under IRB approval. A total of 25 patients were assigned, but three patients did not shown up on the day of collection. Thus, a total of 16 from adult patients

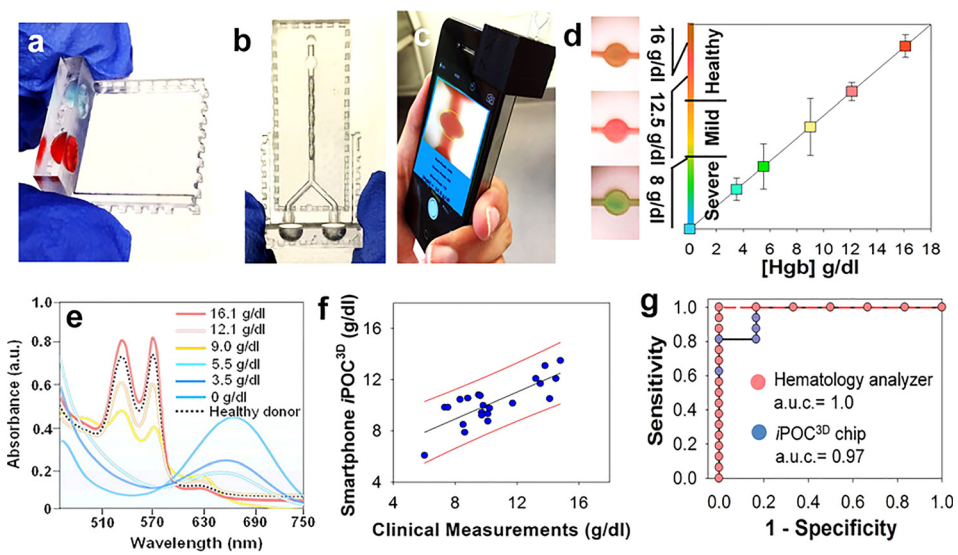

FIG. 5. (a) 3D printed sampling platform. (b) Consistent introduction of blood with oxidizing agents for colorimetric assay. (c) Smartphone sensing system with color-scale analytical app written in-house. (d) Quantitative measurement of Hgb levels for color-scale anemia diagnosis using smartphone *i*POC^{3D} system *via* capillary-driven auto-mixing of finger-prick blood. The calibration curve is established by measuring standard hemoglobin proteins spiked in 100-time diluted blood in 0, 5.5, 8.0, 9.0, 12.5, and 16.0 g/dl, and correlated with color scale. (e) Spectrophotometric analysis of Hgb levels in blood reaction mixture for validating readout from smartphone *i*POC^{3D} system; Hgb peaks are at 540 nm and 575 nm, and TMB peak is at 630 nm. Blood from a healthy donor is indicated in the black dashed line. (f) Pilot study of anemia diagnosis ($n_{anemia} = 16$ and $n_{healthy} = 6$) and the correlation of smartphone *i*POC^{3D} measurements with clinical standard hematology analyzer measurements using Durbin–Watson Statistic Normality test with 95% confidence interval ($r = 0.8$ and $p < 0.0001$). (g) ROC analysis of diagnostic accuracy using smartphone *i*POC^{3D} system, compared with standard clinical measurements using hematology analyzer.

TABLE I. The diagnostic sensitivity and specificity comparison between standard clinical measurements, smartphone-based iPOC3D measurements, and the reported method.

	Standard clinical meas.		Smartphone-based *i*POC^{3D} meas.		Reported method[37]	
Anemia status	Spe.	Sen.	Spe.	Sen.	Spe.	Sen.
Severe anemia	100%	87.5%	100%	81.2%	93.9%	100%
Mild anemia	83.7%	100%	83.3%	100%	91.1%	79.2%

and 6 from healthy donors in outpatient clinics of the University of Kansas Hospital and Biorepository were collected and analyzed using both standard hemotology analyzer and smartphone *i*POC^{3D} system. Fig. 5(f) demonstrated the capability of *i*POC^{3D} system for diagnosing clinical blood samples from anemic patients and healthy individuals, which showed high correlation between clinical measurements and our smartphone *i*POC^{3D} measurements ($r = 0.8$ and $p < 0.0001$). Blood from healthy donors showed Hgb levels in line with the WHO-recommended cutoff (>12 g/dl) (Table S1 of the supplementary material). Severe anemia (<8 g/dl) and mild anemia (<12 g/dl and >8 g/dl) can be clearly differentiated in distinctive color readout. Based on color RGB analysis via an app written in house, direct output of Hgb levels from a smartphone can prevent potential variations due to human color vision, thereby it is suitable for color-blind patients. The diagnostic accuracy of smartphone *i*POC^{3D} system with the area under ROC curve (a.u.c.) is 0.97, which is comparable with standard clinical measurements (a.u.c. = 1.0) (Fig. 5(g) and Table S2 of the supplementary material). Smartphone *i*POC^{3D} system for detecting anemia gives the coefficient of variation in the range of ~0.2%−5% which is less than 0.4 g/dl Hgb (Fig. S2 of the supplementary material). The diagnostic sensitivity is 81.2% for detecting severe anemia, and 100% for mild anemia. The diagnostic specificity is 100% for detecting severe anemia and 83.3% for mild anemia (Table I), yielding comparable diagnostic sensitivity and specificity with standard clinical measurements and reported POC test.[37] These data highlighted the clinical usability of smartphone *i*POC^{3D} system for diagnosing anemia.

CONCLUSIONS

We implemented 3D microfluidic simulation-guided computer design for developing capillary-force enabled auto-mixing in the 3D printed microfluidic chip. Without requiring external power or pump, auto-mixing of oxidizing agents with blood in the micromixer was achieved in 1 s, thereby allowing the development of finger prick blood-based assay for POC diagnosis of anemia, combining with the smartphone as colorimetric sensing platform. The correlation analysis between *i*POC^{3D} measurements and standard clinical measurements showed a significance of $p < 0.0001$ and a correlation coefficient of $r = 0.8$, demonstrating good diagnostic capability. A desktop 3D printer costs ~$4000 with a resin cartridge (~$45) for producing more than 100 chips. The overall cost per test is ~50 cents that covers resin consumed and oxidizing agents. Once the design is optimized and proven proof-of-concept, the manufacturing-scale 3D printer can be used for mass production without requirement of specialized infrastructure. Such low-cost *i*POC^{3D} diagnostic strategy integrates design, fabrication, and disease management in one process as a stand-alone system, offering strong adaptability for establishing diagnostic capacity in resource-limited areas and low-income countries. Set as a pilot study, we will continue to seek coherent large-scale clinical study for validating clinical usability, as well as the efficacy as an anemia screening tool. Although this pilot study focuses on POC diagnosis of anemia, the strong adaptability enables the development of other blood-based diagnostic tests, representing a novel research and diagnostic model.

SUPPLEMENTARY MATERIAL

See supplementary material for details of the parameters of Computational Fluid Dynamics (CFD) simulation, the influence of variable contact angles and contact angle measurement

conditions, clinical patient sample collection, and parameters of diagnostic ROC, specificity, and sensitivity analysis.

ACKNOWLEDGMENTS

We acknowledge the funding support from NIH NIGMS P20 GM103418, K-State Terry C. Johnson Cancer Research Center, and K-State Research Foundation. We thank Professor Steven Warren and Mr. Ethan Grother in the Electrical and Computer Engineering Department at Kansas State University for developing the smartphone color-scale analytical app. We also thank the University of Kansas Hospital and the University of Kansas Medical Center Biorepository for providing clinical blood samples and assisting in blood sample collection and measurement.

[1]P. K. Drain, E. P. Hyle, F. Noubary, K. A. Freedberg, D. Wilson, W. R. Bishai, W. Rodriguez, and I. V. Bassett, "Diagnostic point-of-care tests in resource-limited settings," Lancet Infect. Dis. **14**(3), 239–49 (2014).
[2]L. Xu, H. Lee, M. V. Brasil Pinheiro, P. Schneider, D. Jetta, and K. W. Oh, "Phaseguide-assisted blood separation microfluidic device for point-of-care applications," Biomicrofluidics **9**(1), 014106 (2015).
[3]S. T. Sanjay, M. Dou, J. Sun, and X. Li, "A paper/polymer hybrid microfluidic microplate for rapid quantitative detection of multiple disease biomarkers," Sci. Rep. **6**, 30474 (2016).
[4]M. Dou, J. Lopez, M. Rios, O. Garcia, C. Xiao, M. Eastman, and X. Li, "A fully battery-powered inexpensive spectrophotometric system for high-sensitivity point-of-care analysis on a microfluidic chip," Analyst **141**(12), 3898–3903 (2016).
[5]M. Mohammadi, H. Madadi, and J. Casals-Terre, "Microfluidic point-of-care blood panel based on a novel technique: Reversible electroosmotic flow," Biomicrofluidics **9**(5), 054106 (2015).
[6]C. I. Rogers, K. Qaderi, A. T. Woolley, and G. P. Nordin, "3D printed microfluidic devices with integrated valves," Biomicrofluidics **9**(1), 016501 (2015).
[7]P. K. Yuen, "Embedding objects during 3D printing to add new functionalities," Biomicrofluidics **10**(4), 044104 (2016).
[8]P. F. O'Neill, A. Ben Azouz, M. Vazquez, J. Liu, S. Marczak, Z. Slouka, H. C. Chang, D. Diamond, and D. Brabazon, "Advances in three-dimensional rapid prototyping of microfluidic devices for biological applications," Biomicrofluidics **8**(5), 052112 (2014).
[9]J. Zhou, A. V. Ellis, and N. H. Voelcker, "Recent developments in PDMS surface modification for microfluidic devices," Electrophoresis **31**(1), 2–16 (2010).
[10]J. Friend and L. Yeo, "Fabrication of microfluidic devices using polydimethylsiloxane," Biomicrofluidics **4**(2), 026502 (2010).
[11]Y. Xia, J. Si, and Z. Li, "Fabrication techniques for microfluidic paper-based analytical devices and their applications for biological testing: A review," Biosens. Bioelectron. **77**, 774–89 (2016).
[12]X. Li, D. R. Ballerini, and W. Shen, "A perspective on paper-based microfluidics: Current status and future trends," Biomicrofluidics **6**(1), 11301 (2012).
[13]A. I. Shallan, P. Smejkal, M. Corban, R. M. Guijt, and M. C. Breadmore, "Cost-effective three-dimensional printing of visibly transparent microchips within minutes," Anal. Chem. **86**(6), 3124–30 (2014).
[14]Q. L. Chen, Z. Liu, and H. C. Shum, "Three-dimensional printing-based electro-millifluidic devices for fabricating multicompartment particles," Biomicrofluidics **8**(6), 064112 (2014).
[15]S. J. Keating, M. I. Gariboldi, W. G. Patrick, S. Sharma, D. S. Kong, and N. Oxman, "3D Printed Multimaterial Microfluidic Valve," PLoS One **11**(8), e0160624 (2016).
[16]A. Urrios, C. Parra-Cabrera, N. Bhattacharjee, A. M. Gonzalez-Suarez, L. G. Rigat-Brugarolas, U. Nallapatti, J. Samitier, C. A. DeForest, F. Posas, J. L. Garcia-Cordero, and A. Folch, "3D-printing of transparent bio-microfluidic devices in PEG-DA," Lab Chip **16**(12), 2287–94 (2016).
[17]F. Zhu, J. Skommer, N. P. Macdonald, T. Friedrich, J. Kaslin, and D. Wlodkowic, "Three-dimensional printed millifluidic devices for zebrafish embryo tests," Biomicrofluidics **9**(4), 046502 (2015).
[18]J. A. Kim, H. N. Kim, S. K. Im, S. Chung, J. Y. Kang, and N. Choi, "Collagen-based brain microvasculature model *in vitro* using three-dimensional printed template," Biomicrofluidics **9**(2), 024115 (2015).
[19]I. S. Kinstlinger and J. S. Miller, "3D-printed fluidic networks as vasculature for engineered tissue," Lab Chip **16**(11), 2025–2043 (2016).
[20]L. Zhang, R. N. Deraney, and A. Tripathi, "Adsorption and isolation of nucleic acids on cellulose magnetic beads using a three-dimensional printed microfluidic chip," Biomicrofluidics **9**(6), 064118 (2015).
[21]S. Waheed, J. M. Cabot, N. P. Macdonald, T. Lewis, R. M. Guijt, B. Paull, and M. C. Breadmore, "3D printed microfluidic devices: enablers and barriers," Lab Chip **16**(11), 1993–2013 (2016).
[22]N. Bhattacharjee, A. Urrios, S. Kang, and A. Folch, "The upcoming 3D-printing revolution in microfluidics," Lab Chip **16**(10), 1720–1742 (2016).
[23]A. K. Au, W. Huynh, L. F. Horowitz, and A. Folch, "3D-Printed Microfluidics," Angew. Chem. Int. Ed. Engl. **55**(12), 3862–3881 (2016).
[24]N. Nivedita and I. Papautsky, "Continuous separation of blood cells in spiral microfluidic devices," Biomicrofluidics **7**(5), 54101 (2013).
[25]Y. S. Ho Nam Chan, B. Xiong, Y. Chen, Y. Chen, Q. Tian, S. A. Michael, B. Shen, and H. Wu, "Simple, cost-effective 3D printed microfluidic components for disposable, point-of-care colorimetric analysis," ACS Sens. **1**(3), 227–234 (2016).
[26]A. Chen, R. Wang, C. R. Bever, S. Xing, B. D. Hammock, and T. Pan, "Smartphone-interfaced lab-on-a-chip devices for field-deployable enzyme-linked immunosorbent assay," Biomicrofluidics **8**(6), 064101 (2014).

[27]M. Zangheri, L. Cevenini, L. Anfossi, C. Baggiani, P. Simoni, F. Di Nardo, and A. Roda, "A simple and compact smartphone accessory for quantitative chemiluminescence-based lateral flow immunoassay for salivary cortisol detection," Biosens. Bioelectron. **64**, 63–8 (2015).
[28]B. Berg, B. Cortazar, D. Tseng, H. Ozkan, S. Feng, Q. Wei, R. Y. Chan, J. Burbano, Q. Farooqui, M. Lewinski, D. Di Carlo, O. B. Garner, and A. Ozcan, "Cellphone-based hand-held microplate reader for point-of-care testing of enzyme-linked immunosorbent assays," ACS Nano **9**(8), 7857–7866 (2015).
[29]W. R. A. Eleonora Petryayeva, "A job for quantum dots: use of a smartphone and 3D-printed accessory for all-in-one excitation and imaging of photoluminescence," Anal. Bioanal. Chem. **408**(11), 2913–2925 (2016).
[30]G. Comina, A. Suska, and D. Filippini, "Autonomous chemical sensing interface for universal cell phone readout," Angew. Chem. Int. Ed. Engl. **54**(30), 8708–8712 (2015).
[31]G. Comina, A. Suska, and D. Filippini, "Towards autonomous lab-on-a-chip devices for cell phone biosensing," Biosens. Bioelectron. **77**, 1153–1167 (2016).
[32]K. Yang, H. Peretz-Soroka, Y. Liu, and F. Lin, "Novel developments in mobile sensing based on the integration of microfluidic devices and smartphones," Lab Chip **16**(6), 943–958 (2016).
[33]G. A. Stevens, M. M. Finucane, L. M. De-Regil, C. J. Paciorek, S. R. Flaxman, F. Branca, J. P. Pena-Rosas, Z. A. Bhutta, M. Ezzati, and N. I. M. S. Group, "Global, regional, and national trends in haemoglobin concentration and prevalence of total and severe anaemia in children and pregnant and non-pregnant women for 1995-2011: A systematic analysis of population-representative data," Lancet Global Health **1**(1), E16–E25 (2013).
[34]O. Ngesa and H. Mwambi, "Prevalence and risk factors of anaemia among children aged between 6 months and 14 years in Kenya," PLoS One **9**(11), e113756 (2014).
[35]T. D. Johnson-Wimbley and D. Y. Graham, "Diagnosis and management of iron deficiency anemia in the 21st century," Ther. Adv. Gastroenterol. **4**(3) 177–184 (2011).
[36]M. Corradino, P. H. Whitley, L. Linda, S. J. Graminske, T. Straus, and L. A. Maes, "Noninvasive and invasive point-of-care hemoglobin testing for blood donor qualification," Vox Sang. **105**, 110–110 (2013).
[37]E. A. Tyburski, S. E. Gillespie, W. A. Stoy, R. G. Mannino, A. J. Weiss, A. F. Siu, R. H. Bulloch, K. Thota, A. Cardenas, W. Session, H. J. Khoury, S. O'Connor, S. T. Bunting, J. Boudreaux, C. R. Forest, M. Gaddh, T. Leong, L. A. Lyon, and W. A. Lam, "Disposable platform provides visual and color-based point-of-care anemia self-testing," J. Clin. Invest. **124**(10), 4387–4394 (2014).
[38]N. Ichikawa, K. Hosokawa, and R. Maeda, "Interface motion of capillary-driven flow in rectangular microchannel," J. Colloid Interface Sci. **280**(1), 155–164 (2004).
[39]C. C. Lai and C. K. Chung, "Numerical simulation of the capillary flow in the meander microchannel," Microsyst. Technol. **19**(3), 379–386 (2013).
[40]N. Ichikawa and Y. Satoda, "Interface dynamics of capillary-flow in a tube under negligible gravity condition," J. Colloid Interface Sci. **162**(2), 350–355 (1994).
[41]M. Tani, R. Kawano, K. Kamiya, and K. Okumura, "Towards combinatorial mixing devices without any pumps by open-capillary channels: Fundamentals and applications," Sci. Rep. **5**, 10263 (2015).
[42]T. Scherr, S. Pursley, W. T. Monroe, and K. Nandakumar, "A numerical study on distributions during cryoprotectant loading caused by laminar flow in a microchannel," Biomicrofluidics **7**(2), 24104 (2013).
[43]F. Shen, X. Li, and P. C. Li, "Study of flow behaviors on single-cell manipulation and shear stress reduction in microfluidic chips using computational fluid dynamics simulations," Biomicrofluidics **8**(1), 014109 (2014).
[44]S. W. Lee, D. S. Kim, S. S. Lee, and T. H. Kwon, "A split and recombination micromixer fabricated in a PDMS three-dimensional structure," J. Micromech. Microeng. **16**(5), 1067–1072 (2006).
[45]C. Y. Lee, C. L. Chang, Y. N. Wang, and L. M. Fu, "Microfluidic mixing: A review," Int. J. Mol. Sci. **12**(5), 3263–3287 (2011).
[46]S. Kim, R. A. Bowen, and R. N. Zare, "Transforming plastic surfaces with electrophilic backbones from hydrophobic to hydrophilic," ACS Appl. Mater. Interfaces **7**(3), 1925–1931 (2015).
[47]Y. Isik-Balci, H. Tancer-Elci, M. Bor-Kucukatay, O. Kilic-Erkek, E. Kilic-Toprak, H. Senol, and S. Rota, "Investigation of hemorheological parameters at the diagnosis and follow up of children with iron deficiency anemia and mixed anemia," Clin. Hemorheol. Microcirc. **60**(2), 179–189 (2015).
[48]M. Karagulle, E. Gunduz, F. S. Mutlu, and M. O. Akay, "Clinical significance of reticulocyte hemoglobin content in the diagnosis of iron deficiency anemia," Turk. J. Hematol. **30**(2), 153–156 (2013).
[49]E. Lenters-Westra and R. J. Slingerland, "Three of 7 hemoglobin A(1c) point-of-care instruments do not meet generally accepted analytical performance criteria," Clin. Chem. **60**(8), 1062–1072 (2014).
[50]T. Guo, R. Patnaik, K. Kuhlmann, A. J. Rai, and S. K. Sia, "Smartphone dongle for simultaneous measurement of hemoglobin concentration and detection of HIV antibodies," Lab Chip **15**(17), 3514–20 (2015).
[51]M. Munoz, A. Romero, J. F. Gomez, A. Manteca, E. Naveira, and G. Ramirez, "Utility of point-of-care haemoglobin measurement in the HemoCue-B haemoglobin for the initial diagnosis of anaemia," Clin. Lab. Haematol. **27**(2), 99–104 (2005).
[52]W. L. Ng, T. G. Short, K. N. Gunn, G. S. Fuge, and B. Slon, "Accuracy and reliability of the i-STAT point-of-care device for the determination of haemoglobin concentration before and after major blood loss," Anaesth. Intensive Care **42**(4), 495–499 (2014).
[53]V. A. Skelton, N. Wijayasinghe, S. Sharafudeen, A. Sange, N. S. Parry, and C. Junghans, "Evaluation of point-of-care haemoglobin measuring devices: a comparison of Radical-7 pulse co-oximetry, Hemocue and laboratory measurements in obstetric patients (vol 68, pg 40, 2013)," Anaesthesia **68**(5), 547–548 (2013).
[54]X. X. Yang, N. Z. Piety, S. M. Vignes, M. S. Benton, J. Kanter, and S. S. Shevkoplyas, "Simple paper-based test for measuring blood hemoglobin concentration in resource-limited settings," Clin. Chem. **59**(10), 1506–1513 (2013).
[55]X. X. Yang, J. Kanter, N. Z. Piety, M. Benton, S. M. Vignes, and S. S. Shevkoplyas, "A simple, rapid, low-cost test for the diagnosis of sickle cell disease using a paper-based hemoglobin solubility assay," Blood **120**(21), 245 (2012).
[56]C. F. Ingram and S. M. Lewis, "Clinical use of WHO haemoglobin colour scale: validation and critique," J. Clin. Pathol. **53**(12), 933–937 (2000).
[57]S. S. Levinson and J. Goldman, "Measuring hemoglobin in plasma by reaction with tetramethylbenzidine," Clin. Chem. **28**(3), 471–474 (1982).